ACS Photonics

Article

Cite This: ACS Photonics 2020, 7, 147−153

pubs.acs.org/journal/apchd5

Formation Rules and Dynamics of Photoinduced $\chi^{(2)}$ Gratings in Silicon Nitride Waveguides

Edgars Nitiss,[†] Tianyi Liu,[†,‡] Davide Grassani,[†] Martin Pfeiffer,[‡] Tobias J. Kippenberg,[‡] and Camille-Sophie Brès*[,†]

[†]Ecole Polytechnique Fédérale de Lausanne, Photonic Systems Laboratory (PHOSL), STI-IEL, Station 11, CH-1015 Lausanne, Switzerland

[‡]Ecole Polytechnique Fédérale de Lausanne, Laboratory of Photonics and Quantum Measurements (LPQM), SB-IPHYS, Station 3, CH-1015 Lausanne, Switzerland

Supporting Information

ABSTRACT: Silicon nitride has emerged as a prominent platform for building photonics integrated circuits. While its nonlinear properties based on third-order effects have been successfully exploited, an efficient second harmonic generation in standard stoichiometric silicon nitride (Si_3N_4) waveguides can also be achieved after all-optical poling, as was recently shown. The root of such a phenomenon has been attributed to the inscription of a self-organized periodic space-charge grating along the waveguide, allowing an effective $\chi^{(2)}$ and automatic quasi-phase-matching of pump and second harmonic. However, the different parameters and their role in increasing the efficiency of the process are still not fully comprehended. In this work, we use optical means to identify the general conditions of mode matching occurring during all-optical poling. The overlap integral between pump and second harmonic optical modes is shown to be the governing parameter in determining the features of the $\chi^{(2)}$ gratings. Two-photon microscopy measurements of the $\chi^{(2)}$ gratings reveal the presence of a secondary periodicity in some of the waveguides used in the study. According to overlap integral simulations, such an effect can occur due to mode mixing in the waveguide bends. From a study of poling dynamics, we observe that poling efficiency and rate increase as a function of optical pump power and waveguide length. However, in order to initiate poling, a critical pump intensity, which is lower for longer waveguides, must be coupled into a waveguide. Temporal and thermal stability tests reveal the nature of charge traps responsible for grating inscription. After applying thermally activated hopping as a conductivity mechanism in our samples, we show that only shallow traps seem to be activated during the all-optical poling process.

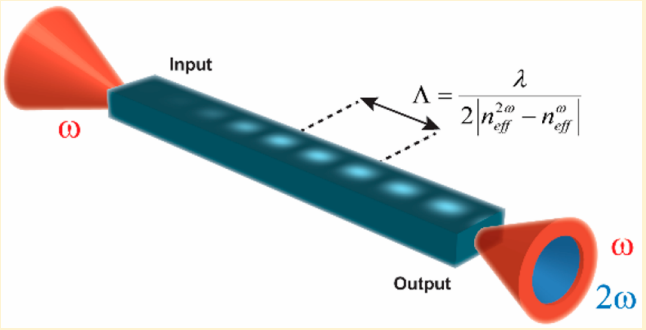

KEYWORDS: *stoichiometric silicon nitride, nonlinear optics, second harmonic generation, all-optical poling, quasi-phase-matching*

Silicon nitride currently is one of the most frequently employed CMOS compatible platforms for building nonlinear photonic integrated circuits. Due to its high third-order ($\chi^{(3)}$) nonlinearity, absence of two-photon absorption throughout the infrared, high refractive index, and low absorption in the visible and infrared spectral regions, stoichiometric silicon nitride (Si_3N_4) waveguides have been demonstrated to be excellent candidates for ultralow loss resonators,[1−3] entangled photon-pair generation,[4] and optical frequency comb generation,[5−7] as well as low pulse energy supercontinuum generation in the near[8] and mid-infrared.[9] Since Si_3N_4 is amorphous it does not exhibit significant second-order ($\chi^{(2)}$) nonlinearity, yet it would be highly desirable for envisioned nonlinear optical applications, including spontaneous parametric down-conversion, second harmonic generation (SHG), and others.

Various methods to induce an effective $\chi^{(2)}$ in Si_3N_4 waveguides have been proposed and demonstrated by either inducing a symmetry breaking at interfaces[10−13] or, as very recently shown, by performing all-optical poling.[14−16] The latter method has up to now resulted in maximum effective $\chi^{(2)}$ in the order of pm/V,[15,17] but offers the advantage of versatility and reconfigurability. Such all-optical poling was demonstrated and extensively studied in SiO_2 optical fibers three decades ago.[18−25] In both the SiO_2 and Si_3N_4 work, it has been recognized that during the all-optical poling process, second-order nonlinearity and quasi-phase-matching (QPM) build up spontaneously due to the coherent photogalvanic effect.[23,26−28] As the waveguide is illuminated by a high intensity pump (at fundamental harmonic, FH), an initial weak second harmonic (SH) seed light is generated from intrinsic nonlinearity at interfaces, material anisotropies, or electric quadrupole interactions.[11,29,30] Within the photogalvanic effect, an interference between multiphoton absorption of FH and SH

Received: September 9, 2019
Published: December 9, 2019

DOI: 10.1021/acsphotonics.9b01301
ACS Photonics 2020, 7, 147−153

takes place at color centers, leading to an asymmetric photocurrent, the photogalvanic current, and subsequent carrier trapping. This creates a self-organized periodic space-charge grating along the waveguide. The product of this frozen electric field and third-order susceptibility works as an effective $\chi^{(2)}$ with the same periodicity of the grating. When using continuous wave (CW) or long pulses pump lasers, the coherent photogalvanic effect has the remarkable property to automatically provide QPM of FH and SH[24,31] without the need to engineer the dispersion of the waveguide. The space-charge separation has been confirmed by localized SH measurement in bulk[28] by selective etching technique in fibers[32] as well as by nonlinear microscopy in waveguides.[16] It is also known that, in the short pulse regime, waveguide dispersion needs to be engineered as to provide the required group-velocity phase-matching to initiate the all-optical poling process,[16] thus, strongly limiting the versatility of the effect, which is constrained to specific waveguide designs.

Despite numerous observations of the effect, several open questions have remained unanswered. First, the relationship between the properties of the grating and waveguide parameters were not clear for cases when the waveguide is poled in the long pulse and continuous wave regime. Such a regime provides the desired versatility and tunability; however, the relationship between grating and waveguide parameters is still not well-defined, mainly due to a controversial and limited number of mode properties and grating observations. All recent work in all-optically poled Si_3N_4 waveguides assumed that modal phase-matching was taking place.[14,15] In such a case, the initial SH would be generated on the waveguide mode that provides the smallest phase mismatch with the pump. This was supported by the observation of higher order SH modes at the output of all-optically poled Si_3N_4 waveguides with bends.[15] However, in early work on all-optical poling of SiO_2 multimode fibers, it was found that the SH would be mostly generated in the fundamental mode of the waveguide,[18,32] thus, providing contradicting information. Second, the stability of the imposed nonlinearity is still not well understood nor quantified, even though it is one of the most important parameters for understanding the all-optical poling process. It is commonly assumed that the traps are long-lived and the $\chi^{(2)}$ grating can be bleached only with high energy photons.[16,33] However, the grating stability that is related to the properties of trap sites that are present in all-optically poled Si_3N_4 waveguides has not yet been investigated in detail.

Here we use optical means to study the properties of $\chi^{(2)}$ gratings. By using two-photon microscopy (TPM), we directly image the optically written grating in waveguides with different geometries and, for the first time, provide the evidence on general conditions of mode matching responsible for grating formation, as well as demonstrate the influence of waveguide parameters on the quality of QPM. It is shown that the process initiates on modes with the highest overlap and not with the smallest phase mismatch, establishing that this all-optical poling can compensate large phase mismatch. Here we also provide an explanation on the occurrence of SH generated on higher order modes. We investigate the temporal dynamics of the $\chi^{(2)}$ grating and the influence of the pump power and waveguide length on the conversion efficiency (CE) defined as $CE = P_{SH}/P_{FH}^2$, with P_{SH} and P_{FH} being the power at the SH and FH, respectively. Finally, we study the stability of $\chi^{(2)}$ grating in time and account for the traps responsible for space charge modulation. These findings establish that, while the dimensions of the waveguide and, thus, the dispersion do not influence the process, the losses and the layout of the waveguide on the chip do have critical importance, as they impact the efficiency and the quality of the grating.

EXPERIMENTAL SETUP

The experimental setup used for all-optical poling of Si_3N_4 waveguides consists in a CW light from a coherent tunable light source shaped by a Mach–Zehnder modulator into pulse trains with arbitrary pulse width at a repetition rate of 5 MHz. The pulses at pump wavelength are amplified using two subsequent amplification and filtering stages, and the peak power in the chips can reach up to 115 W. Light polarization is modified using a fiber-polarizer. The light is then collimated and focused by two optical lenses for coupling to the Si_3N_4 waveguide. The FH and SH light at the output of the waveguide is collected with a 20× microscope objective and delivered to photodetectors. Light reflected by a dichroic beam splitter with cutoff at 1100 nm is delivered to an infrared detector, while the transmitted light is filtered with a set of edge-pass filters. For measuring the SH response as a function of pump wavelength, the pulse shaping stage was bypassed and the output of the chip was directed to an optical spectrum analyzer.

The Si_3N_4 waveguides under test are fabricated according to the photonic Damascene process[34] in three runs. Heights of waveguides are 0.78, 0.81, and 0.87 μm, respectively, and widths varied from 0.57 to 1.9 μm (for more details, see the Supporting Information). The waveguides are folded in meanders on 5 × 10 and 5 × 5 mm^2 chips by using curved sections with a radius of 75 μm and a length spanning from 22.4 to 57.7 mm.

$\chi^{(2)}$ GRATING CHARACTERIZATION

When a high intensity pulsed pump is injected in the waveguide, the SH grows with time due to the formation of a $\chi^{(2)}$ grating, until reaching saturation. The growth time varies in the range of a couple of minutes to several hours (see Figure 1) and is determined by the coupled peak-power, as will be shown latter.

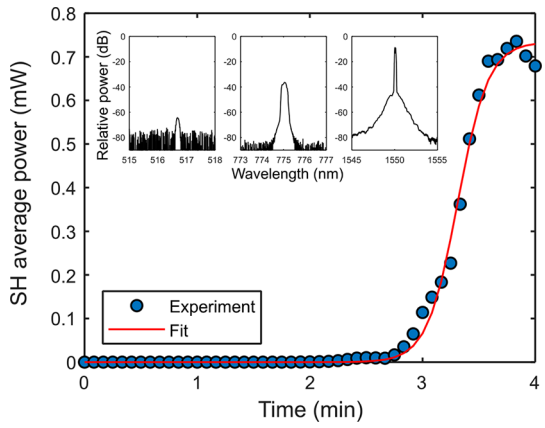

Figure 1. Experimentally measured buildup of average SH as a function of time in a 40 mm long waveguide with dimensions of 1.6 × 0.87 μm^2; pump pulse duration, 1 ns; coupled peak power, 113 W. Experimental points are fitted with a sigmoidal logistic function (type 1). Inset: spectral composition at the chip output consisting of third-harmonic (TH), SH, and FH, respectively.

DOI: 10.1021/acsphotonics.9b01301
ACS Photonics 2020, 7, 147−153

To confirm the presence of a $\chi^{(2)}$ grating, we used two-photon microscopy (TPM) imaging and recorded images of the grating. During a raster-scan, the SH of a 1010 nm pump was collected across the sample (for more details see Supporting Information). The poled waveguide exhibiting SH generation appears bright, as seen in Figure 2a. The

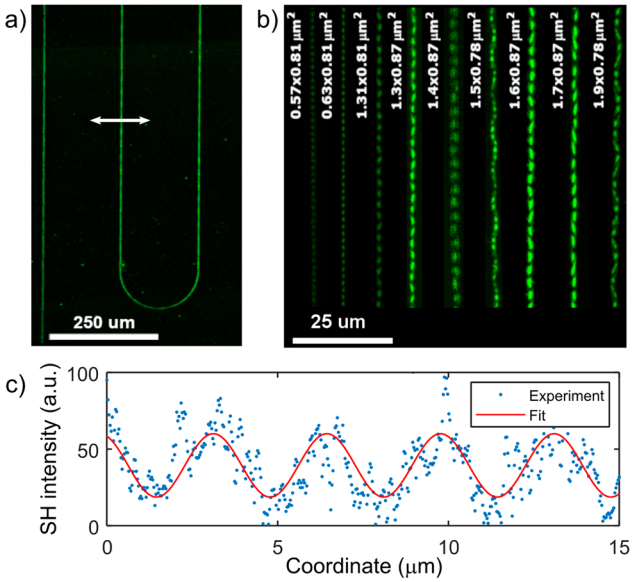

Figure 2. (a) TPM in a poled 40 mm long Si_3N_4 waveguide with cross-section of 1.6 × 0.87 μm^2 using TE polarized 1.55 μm light. White arrow indicates microscopy laser light polarization. (b) TPM images of $\chi^{(2)}$ grating in waveguides with different cross sections. (c) Example of extracted SH intensity along the waveguide with cross-section of 1.7 × 0.87 μm^2.

meanders are clearly visible with the slight loss of intensity in the bends explained by the polarization of the illumination (shown by the white arrow). By zooming in, a periodical SH response along the waveguides is evident and the grating period Λ can be extracted from the images by fitting the SH intensity using a sine-squared function (see Figure 2b,c). According to the theory of photogalvanic effect, the $\chi^{(2)}$ grating period Λ is inversely proportional to the effective index difference of guided FH and SH modes, n_{eff}^{ω} and $n_{eff}^{2\omega}$, respectively:

$$\Lambda = \frac{\lambda}{2|n_{eff}^{2\omega} - n_{eff}^{\omega}|} \quad (1)$$

where λ is the FH wavelength. We calculated the effective indexes of all modes supported by the waveguide using a numerical mode solver.

In Figure 3, we plot the measured $\chi^{(2)}$ grating periods versus simulated values solely based on the interaction of fundamental modes at both the FH and SH wavelengths. The measurements agree well with the simulations for all waveguides except for the 1.5 × 0.78 μm^2 waveguide, for which a much smaller period is retrieved. Therefore, the SH seems to be generated on the fundamental waveguide mode, despite the larger phase mismatch with respect to the case where the SH is generated on higher order modes. To better understand this point, we performed numerical simulations of overlap integrals Γ, which are known to be directly proportional to the mode coupling strength. Indeed, in a straight waveguide Γ between

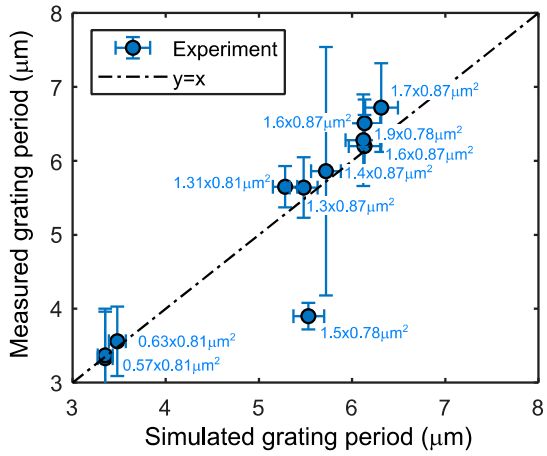

Figure 3. Measured vs simulated $\chi^{(2)}$ grating period in poled waveguides of different dimensions. Vertical error bars indicate the period measurement error, while horizontal error bars indicate simulated grating period error considering fabrication tolerances.

fundamental modes reaches 95% and is several orders of magnitude higher than for any other combinations of modes. This suggests that Γ is the dominant parameter in determining which SH mode will be excited, and sets Λ, as a direct consequence.

In addition, Λ remains constant, within a measurement error margin, throughout the grating length. However, the grating amplitude appears to vary: it is undetectable at the waveguide input then quickly grows and eventually saturates, suggesting sigmoidal shape as also previously observed.[16,19] Finally, it is evident that in some waveguides a weakly pronounced $\chi^{(2)}$ grating is present, leading to a wavy behavior of the grating as seen in Figure 2b, an indication that the energy from the FH is transferred to SH modes other than the fundamental one. This most probably is the result of mode distortions experienced in the waveguide's bends, resulting in increased overlap integrals to higher order modes (for more details, see Supporting Information). Such mode mixing could be the reason for distorted periodicity of the primary grating and introduction of errors in the primary period estimation. For narrow waveguides, such as the ones with 0.57 and 0.63 μm width, the fundamental FH mode is strongly confined and no mode mixing is expected, even in the bends.

In all waveguides poled using a 1.55 μm pump the SH response was subsequently measured through a low power CW wavelength sweep. The results can be divided into two cases, which are illustrated in Figure 4 showing the CE as a function of wavelength in three waveguides with similar length, but different cross-section and poled with the same pump. In the first case (Figure 3a,b), a broadband response is observed with no well-defined phase-matching peak. For some waveguides used in our experiments the highest response is not even located at the poling wavelength. Moreover, when coupling spectrally broad picosecond pulses, we can observe a broad SH response even though group-velocity phase matching is not satisfied. Such observations in QPM measurements is an indication of stochastic variations of the period along the grating length,[35] which could be a consequence of mode mixing. In the other case, the SH response is a narrowband with a sinc-shape (Figure 3c). Such a response occurs solely for the narrow waveguides with widths of 0.57 and 0.63 μm, where no mode mixing is expected.

DOI: 10.1021/acsphotonics.9b01301
ACS Photonics 2020, 7, 147−153

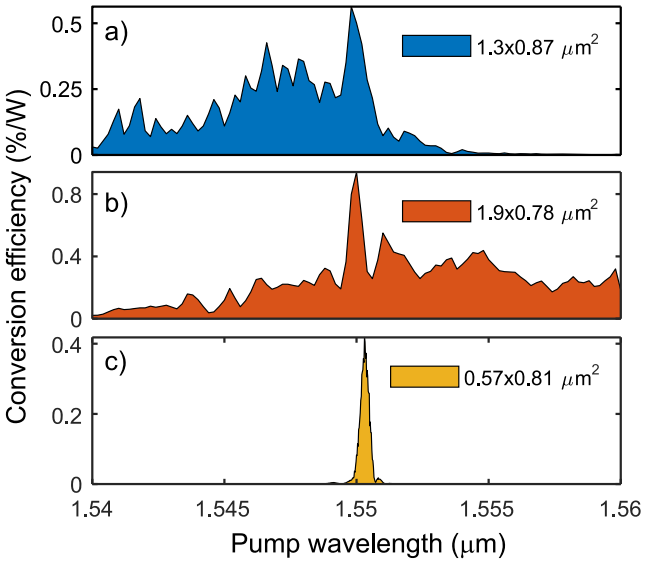

Figure 4. Measured conversion efficiency in %/W as a function of pump wavelength for waveguides poled at 1.55 μm with dimensions (a) 1.3 × 0.87 μm^2, (b) 1.9 × 0.78 μm^2, and (c) 0.57 × 0.81 μm^2.

POLING DYNAMICS

As reported elsewhere, the $\chi^{(2)}$ grating can be erased with high energy photons.[16,33,36] We used this effect to do a systematic study of poling dynamics. We erase the grating by injecting a kW peak power femtosecond laser at 1.56 μm in the waveguides. Due to the propagation of high peak power fs pulses, the generation of high energy photons due to strong TH and visible supercontinuum generation takes place. The supercontinuum generated in the waveguide erases the grating within a couple of seconds, after which the poling procedure can be consistently repeated.

We first investigate the grating properties at different times during poling. The measured CE as a function of time is shown in Figure 5a. The red points correspond to poling interrupts after which TPM measurements were performed as to measure the grating length (see Supporting Information). The CE as a function of grating length is plotted in Figure 5b. We expect the CE to be proportional to the square of grating length, represented by the blue dashed line in Figure 5b for an assumed constant grating amplitude after normalization to the highest value.

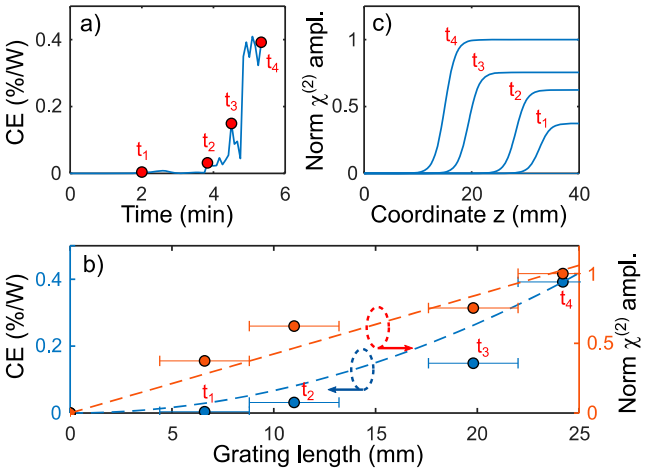

Figure 5. (a) Measured CE during poling in a 40 mm long 1.6 × 0.87 μm^2 waveguide. Points t_1, t_2, t_3, and t_4 are interrupt instants when TPM images are taken. (b) CE and normalized grating amplitude vs measured grating length at each interrupt point. (c) Estimated normalized $\chi^{(2)}$ grating amplitude along waveguide at different poling times.

Owing to the strong deviation between experimental values and such quadratic fit, we can expect that the grating amplitude actually varies during poling. On the secondary y axis in Figure 5b we plot the expected grating amplitude at each interruption point normalized to grating amplitude at maximal reached CE. As can be seen, during poling, the grating amplitude seems to increase linearly simultaneously with grating length, also illustrated in Figure 5c.

The flexibility of our poling setup allows us to easily vary the width of optical pulses and, thus, while maintaining the same average power, to modify the peak power coupled to the waveguides. In Figure 6 we show the trends for maximal CE measured after poling and for SH intensity growth rate as a function of input peak power. We performed the measurements for two waveguides with an identical cross-section of 1.6 × 0.87 μm^2, but different lengths −40 and 22.5 mm, respectively. It should be noted that, while the trend for CE can be retrieved with pulsed pump excitation, we subsequently use CW probing to extract more accurate CE values. Several important observations can be outlined. First, there is a critical input peak power necessary to initiate the poling process. The shorter the waveguide, the higher this critical input peak power. In our waveguides (see Supporting Information), the estimated peak power to initiate poling is of the order of tens of watts, which is consistent with previous observations.[15] Therefore, in order to initiate the poling in an optical waveguide, it must be able to withstand high optical power operation, which can be handled by Si_3N_4. Second, both CE and growth rate are higher for longer waveguides. This could be due to the fact that during all-optical poling the initial SH seed light at the end of the waveguide, where the grating initially builds up, is higher in a longer waveguide. As shown elsewhere, the growth rate and efficiency are larger when more intense seed light is employed.[37,38] Third, the maximal CE and

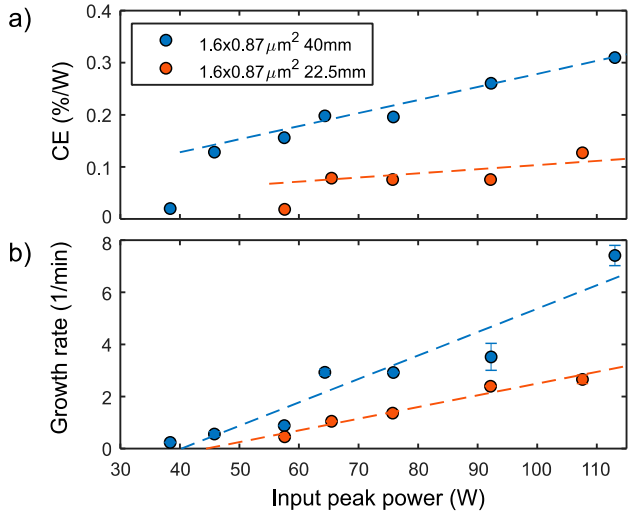

Figure 6. (a) CE during poling and (b) growth rate as a function of input coupled peak power for two waveguides having the same cross-section of 1.6 × 0.87 μm^2, but different lengths −22.5 and 40 mm.

DOI: 10.1021/acsphotonics.9b01301
ACS Photonics 2020, 7, 147−153

growth rate are determined only by the peak power not the average power. This is also confirmed by measurements performed for constant peak power, but increasing pulse duration, and then average power, which results in constant maximal CE and growth rates. It is important to outline that all-optical poling was done in random order so that we would avoid correlations due to memory effects if such were present.

Using a CW probe after poling, the maximal value of CE we extracted from the 40 mm long waveguide is 0.31%/W. The effective $\chi^{(2)}$ is calculated using the following equation:[39]

$$\chi_{\text{eff}}^{(2)} = 2\sqrt{\frac{\eta S_{\text{eff}} \varepsilon_0 c^3 n_\omega^2 n_{2\omega}}{2\omega^2 L^2}} \tag{2}$$

where η is the CE in %/W, n_ω and $n_{2\omega}$ are the effective refractive indexes at FH and SH, respectively, ω is the pump frequency, and L is the grating length. S_{eff} is the effective area calculated as

$$S_{\text{eff}} = \frac{A_{2\omega}}{A_\omega^2} \tag{3}$$

A_ω and $A_{2\omega}$ are the mode areas of the FH and SH wavelength, respectively, defined as

$$A = \int \text{Re}[E_x H_z^* - E_z H_x^*]\,\text{d}x\text{d}z \tag{4}$$

where $E_{x,z}$ and $H_{x,z}$ are the electric and magnetic fields in the corresponding directions, normalized to power flux. Based on the simulated effective area of 0.48 μm^2 and a grating length of 20 mm, $\chi_{\text{eff}}^{(2)}$ is calculated to be of the order of 0.09 pm/V.

TEMPORAL STABILITY

While the grating remains inscribed in the waveguide when the pump is off, we measure a slow decay of SH conversion efficiency in the poled waveguides over a period of several weeks. We assess the thermal stability of the grating through a series of tests performed on the 1.7 × 0.87 μm^2 waveguide. After all-optical poling until saturation of SH CE, the sample was kept on a hot-plate at fixed temperature (21, 100, 150, 175, and 200 °C) and SH CE was measured repeatedly over time with a CW probe. In Figure 7 we plot the decay of normalized CE for high temperature cases, while the inset shows room temperature behavior in days. The CE decay is faster for higher temperatures. The experimental points were fitted assuming thermally activated hopping in a present static electric field, as described in Supporting Information. The calculated average barrier height from the fits is 0.44 ± 0.06 eV.

The obtained value of average barrier height contradicts the common presumption that deep traps are responsible for the capture of charge carriers in all-optically poled Si_3N_4. Indeed, Si_3N_4 has been used in semiconductor memories with long-term stability attributed to the presence of deep traps.[40] It has been suggested that deep traps are positively charged Si defects[41] and are mainly located at interfaces of nitride and oxide where excess silicon is present and their trap energy is around 1.5 eV below the conduction band.[42,43] Yet, our measurement results show that, in the currently employed poling process, only shallow traps seem to be activated. There could be several sources of shallow traps in Si_3N_4, such as the Si dangling bond back bonded to three N atoms ($N_3{\equiv}Si^*$), hydrogen caused trap sites[42,44] or metal impurities that have been observed to be present in the photonic Damascene process used for waveguide preparation.[45]

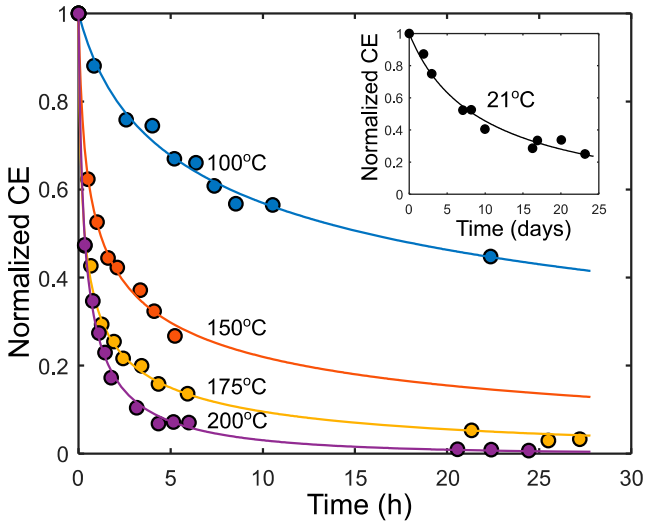

Figure 7. Decay of normalized CE measured at different hot-plate temperatures. Inset: decay at room temperature. Lines are fits based on the model described in the Supporting Information.

DISCUSSION AND CONCLUSIONS

We use all-optical poling to induce self-organized effective $\chi^{(2)}$ gratings in Si_3N_4 waveguides. As shown, the employed all-optical poling approach can be applied to waveguides with arbitrary dimensions, and saturation of nonlinearity can be reached in a time scale of minutes. By using TPM imaging of poled waveguides we measure the period of $\chi^{(2)}$ grating and show that the overlap integral is the dominant parameter that determines to which SH mode the energy will be transferred. This favors SHG on the fundamental waveguide mode, with clear benefits for downstream treatment of the SH signal.

We also observe secondary periodicity of the grating which is attributed to mode mixing in the waveguide bends. This distorted shape of $\chi^{(2)}$ grating causes the spectral response of the poled waveguide to be broadband implying a stochastic variation of grating period along the waveguide. This effect is confirmed by the phase-matching measurements performed in narrow waveguides in which mode mixing is not expected to occur. For this case, the SH response is indeed narrowband with the expected sinc-shaped response.

The all-optical poling can be described using a phenomenological model detailed in Supporting Information and is attributed to the photogalvanic effect.[23,27,28] Charge transport is taking place via electron hopping from one trap to another in the presence of FH and SH. Such model implies that a critical electric field, from the interference of FH and SH, is necessary in order to initiate the charge hopping and, hence, the all-optical poling process as evident from Figure 6. We also observe that the maximal reachable CE during poling is greater when higher pump power is used. Indeed higher photoinduced poling fields would result in longer gratings with larger amplitudes. The grating length and amplitude are determined by a combination of multiple factors. While higher FH and SH intensities would increase both values, light at any other frequency would distort the poling field inside the waveguide. The drawback of using high intensity pump is thus the unavoidable presence of TH. The TH is counteracting the $\chi^{(2)}$

DOI: 10.1021/acsphotonics.9b01301
ACS Photonics 2020, 7, 147−153

grating growth and could be one of the reasons why the grating formation near the input of waveguide is never observed. We expect that by still increasing the pump intensity we would be able to achieve higher CE in our waveguides, until the TH or other frequencies generated due to nonlinear effects would quench the $\chi^{(2)}$ grating formation.

After performing a series of temporal and thermal stability tests, we demonstrate that the grating can be bleached also by heating. Using thermally activated hopping as a conductivity mechanism in our samples, we show that only shallow traps with an average energy of 0.44 eV seem to be activated in the poling process used here. There could be several approaches for both enhancing the nonlinearity as well as increasing its stability, as suggested by results of studies on poled optical glasses. An early work in poled glasses has demonstrated that the stability can be increased by introducing small concentration of dopants in the waveguide.[46] Here, the dopants introduce traps that are more permanent, causing the average trap energy to increase. Alternative approaches include providing thermal or optical energy during poling which results in reduction of conductivity as well as activation of deeper traps beneficial to poling efficiency and stability. For example, thermally assisted poling has long been used in both inorganic[47] and organic glasses.[48,49] Alternatively, UV-assisted poling has shown to lead to higher efficiencies[50,51] as well as a significant increase in the lifetime of induced nonlinearity.[52]

■ ASSOCIATED CONTENT

Supporting Information

The Supporting Information is available free of charge at https://pubs.acs.org/doi/10.1021/acsphotonics.9b01301.

Sample description, numerical simulations of effective refractive indexes and overlap integrals, charge transport model, and nonlinearity decay fit (PDF)

■ AUTHOR INFORMATION

Corresponding Author

*E-mail: camille.bres@epfl.ch.

ORCID

Edgars Nitiss: 0000-0001-9577-9958

Notes

The authors declare no competing financial interest.

■ ACKNOWLEDGMENTS

The funding was provided by ERC Grant PISSARRO (ERC-2017-CoG 771647). The authors also acknowledge the support provided by LIGENTEC and VLC Photonics on the design and manufacturing of the PICs described in this paper.

■ REFERENCES

(1) Xuan, Y.; Liu, Y.; Varghese, L. T.; Metcalf, A. J.; Xue, X.; Wang, P.-H.; Han, K.; Jaramillo-Villegas, J. A.; Al Noman, A.; Wang, C.; et al. High-Q Silicon Nitride Microresonators Exhibiting Low-Power Frequency Comb Initiation. *Optica* **2016**, *3* (11), 1171−1180.

(2) Liu, J.; Raja, A. S.; Karpov, M.; Ghadiani, B.; Pfeiffer, M. H. P.; Du, B.; Engelsen, N. J.; Guo, H.; Zervas, M.; Kippenberg, T. J. Ultralow-Power Chip-Based Soliton Microcombs for Photonic Integration. *Optica* **2018**, *5* (10), 1347−1353.

(3) Ji, X.; Barbosa, F. A. S.; Roberts, S. P.; Dutt, A.; Cardenas, J.; Okawachi, Y.; Bryant, A.; Gaeta, A. L.; Lipson, M. Ultra-Low-Loss on-Chip Resonators with Sub-Milliwatt Parametric Oscillation Threshold. *Optica* **2017**, *4* (6), 619−624.

(4) Ramelow, S.; Farsi, A.; Clemmen, S.; Orquiza, D.; Luke, K.; Lipson, M.; Gaeta, A. L. Silicon-Nitride Platform for Narrowband Entangled Photon Generation. *arXiv:1508.04358* **2015**, na.

(5) Kippenberg, T. J.; Holzwarth, R.; Diddams, S. A. Microresonator-Based Optical Frequency Combs. *Science* **2011**, *332*, 555−559.

(6) Gaeta, A. L.; Lipson, M.; Kippenberg, T. J. Photonic-Chip-Based Frequency Combs. *Nat. Photonics* **2019**, *13* (3), 158−169.

(7) Guo, H.; Herkommer, C.; Billat, A.; Grassani, D.; Zhang, C.; Pfeiffer, M. H. P.; Weng, W.; Brès, C.-S.; Kippenberg, T. J. Mid-Infrared Frequency Comb via Coherent Dispersive Wave Generation in Silicon Nitride Nanophotonic Waveguides. *Nat. Photonics* **2018**, *12* (6), 330−335.

(8) Johnson, A. R.; Mayer, A. S.; Klenner, A.; Luke, K.; Lamb, E. S.; Lamont, M. R. E.; Joshi, C.; Okawachi, Y.; Wise, F. W.; Lipson, M.; et al. Octave-Spanning Coherent Supercontinuum Generation in a Silicon Nitride Waveguide. *Opt. Lett.* **2015**, *40* (21), 5117−5120.

(9) Grassani, D.; Tagkoudi, E.; Guo, H.; Herkommer, C.; Yang, F.; Kippenberg, T. J.; Brès, C.-S. Mid Infrared Gas Spectroscopy Using Efficient Fiber Laser Driven Photonic Chip-Based Supercontinuum. *Nat. Commun.* **2019**, *10* (1), 1553.

(10) Lettieri, S.; Finizio, S. Di; Maddalena, P.; Ballarini, V.; Giorgis, F. Second-Harmonic Generation in Amorphous Silicon Nitride Microcavities. *Appl. Phys. Lett.* **2002**, *81* (25), 4706−4708.

(11) Levy, J. S.; Foster, M. A.; Gaeta, A. L.; Lipson, M. Harmonic Generation in Silicon Nitride Ring Resonators. *Opt. Express* **2011**, *19* (12), 11415−11421.

(12) Ning, T.; Pietarinen, H.; Hyvärinen, O.; Kumar, R.; Kaplas, T.; Kauranen, M.; Genty, G. Efficient Second-Harmonic Generation in Silicon Nitride Resonant Waveguide Gratings. *Opt. Lett.* **2012**, *37* (20), 4269−4271.

(13) Castellan, C.; Trenti, A.; Vecchi, C.; Marchesini, A.; Mancinelli, M.; Ghulinyan, M.; Pucker, G.; Pavesi, L. On the Origin of Second Harmonic Generation in Silicon Waveguides with Silicon Nitride Cladding. *Sci. Rep.* **2019**, *9* (1), 1088.

(14) Billat, A.; Grassani, D.; Pfeiffer, M. H. P.; Kharitonov, S.; Kippenberg, T. J.; Brès, C. S. Large Second Harmonic Generation Enhancement in Si_3N_4 Waveguides by All-Optically Induced Quasi-Phase-Matching. *Nat. Commun.* **2017**, *8* (1), 1016.

(15) Porcel, M. A. G.; Mak, J.; Taballione, C.; Schermerhorn, V. K.; Epping, J. P.; van der Slot, P. J. M.; Boller, K.-J. Photo-Induced Second-Order Nonlinearity in Stoichiometric Silicon Nitride Waveguides. *Opt. Express* **2017**, *25* (26), 33143−33159.

(16) Hickstein, D. D.; Carlson, D. R.; Mundoor, H.; Khurgin, J. B.; Srinivasan, K.; Westly, D.; Kowligy, A.; Smalyukh, I. I.; Diddams, S. A.; Papp, S. B. Self-Organized Nonlinear Gratings for Ultrafast Nanophotonics. *Nat. Photonics* **2019**, *13* (7), 494−499.

(17) Grassani, D.; Pfeiffer, M. H. P.; Kippenberg, T. J.; Brès, C.-S. Second- and Third-Order Nonlinear Wavelength Conversion in an All-Optically Poled Si3N4 Waveguide. *Opt. Lett.* **2019**, *44* (1), 106−109.

(18) Österberg, U.; Margulis, W. Dye Laser Pumped by Nd:YAG Laser Pulses Frequency Doubled in a Glass Optical Fiber. *Opt. Lett.* **1986**, *11* (8), 516−518.

(19) Österberg, U.; Margulis, W. Experimental Studies on Efficient Frequency Doubling in Glass Optical Fibers. *Opt. Lett.* **1987**, *12* (1), 57−59.

(20) Margulis, W.; Österberg, U. Second-Harmonic Generation in Optical Glass Fibers. *J. Opt. Soc. Am. B* **1988**, *5* (2), 312−316.

(21) Valk, B.; Kim, E. M.; Salour, M. M. Second Harmonic Generation in Ge-Doped Fibers with a Mode-Locked Kr + Laser. *Appl. Phys. Lett.* **1987**, *51* (10), 722−724.

(22) Farries, M. C.; Russell, P. S. J.; Fermann, M. E.; Payne, D. N. Second-Harmonic Generation in an Optical Fibre by Self-Written $\chi(2)$ Grating. *Electron. Lett.* **1987**, *23* (7), 322−324.

(23) Anderson, D. Z.; Mizrahi, V.; Sipe, J. E. Model for Second-Harmonic Generation in Glass Optical Fibers Based on Asymmetric Photoelectron Emission from Defect Sites. *Opt. Lett.* **1991**, *16* (11), 796−798.

DOI: 10.1021/acsphotonics.9b01301
ACS Photonics 2020, 7, 147−153

(24) Stolen, R. H.; Tom, H. W. K. Self-Organized Phase-Matched Harmonic Generation in Optical Fibers. *Opt. Lett.* **1987**, *12* (8), 585−587.
(25) Tom, H. W. K.; Stolen, R. H.; Aumiller, G. D.; Pleibel, W. Preparation of Long-Coherence-Length Second-Harmonic-Generating Optical Fibers by Using Mode-Locked Pulses. *Opt. Lett.* **1988**, *13* (6), 512−514.
(26) Baskin, É. M.; Éntin, M. V. Coherent Photovoltaic Effect Due to the Quantum Corrections. *J. Exp. Theor. Phys. Lett.* **1988**, *48*, 601−603.
(27) Baranova, N. B.; Zel'dovich, B. Y.; Chudinov, A. N.; Shul'ginov, A. A. Theory and Observation of Polar Asymmetry of Photoionization in a Field with $\langle E^3 \rangle \neq 0$. *Zh. Eksp. Teor. Fiz.* **1990**, *98*, 1857−1868.
(28) Dianov, E. M.; Starodubov, D. S. Photoinduced Generation of the Second Harmonic in Centrosymmetric Media. *Quantum Electron.* **1995**, *25* (5), 395−407.
(29) Terhune, R. W.; Weinberger, D. A. Second-Harmonic Generation in Fibers. *J. Opt. Soc. Am. B* **1987**, *4* (5), 661−674.
(30) Koskinen, K.; Czaplicki, R.; Slablab, A.; Ning, T.; Hermans, A.; Kuyken, B.; Mittal, V.; Murugan, G. S.; Niemi, T.; Baets, R.; et al. Enhancement of Bulk Second-Harmonic Generation from Silicon Nitride Films by Material Composition. *Opt. Lett.* **2017**, *42* (23), 5030−5033.
(31) Mizrahi, V.; Hibino, Y.; Stegeman, G. Polarization Study of Photoinduced Second-Harmonic Generation in Glass Optical Fibers. *Opt. Commun.* **1990**, *78* (3−4), 283−288.
(32) Margulis, W.; Laurell, F.; Lesche, B. Imaging the Nonlinear Grating in Frequency-Doubling Fibres. *Nature* **1995**, *378* (6558), 699−701.
(33) Ouellette, F.; Hill, K. O.; Johnson, D. C. Light-Induced Erasure of Self-Organized $\chi(2)$ Gratings in Optical Fibers. *Opt. Lett.* **1988**, *13* (6), 515−517.
(34) Pfeiffer, M. H. P.; Kordts, A.; Brasch, V.; Zervas, M.; Geiselmann, M.; Jost, J. D.; Kippenberg, T. J. Photonic Damascene Process for Integrated High-Q Microresonator Based Nonlinear Photonics. *Optica* **2016**, *3* (1), 20−25.
(35) Helmfrid, S.; Arvidsson, G. Influence of Randomly Varying Domain Lengths and Nonuniform Effective Index on Second-Harmonic Generation in Quasi-Phase-Matching Waveguides. *J. Opt. Soc. Am. B* **1991**, *8* (4), 797−804.
(36) Balakirev, M. K.; Vostrikova, L. I.; Smirnov, V. A.; Éntin, M. V. Relaxation of the Optical Density of Glass Modulated with Bichromatic Radiation. *JETP Lett.* **1996**, *63* (3), 176−181.
(37) Batdorf, B.; Krautschik, C.; Österberg, U.; Stegeman, G.; Leitch, J. W.; Rotgé, J. R.; Morse, T. F. Study of the Length Dependence of Frequency-Doubled Light in Optical Fibers. *Opt. Commun.* **1989**, *73* (5), 393−397.
(38) Krol, D. M.; Stolen, R. H.; Tom, H. W. K.; Broer, M. M.; Nelson, K. T.; Pleibel, W. Seeded Second-Harmonic Generation in Optical Fibers: The Effect of Phase Fluctuations. *Opt. Lett.* **1991**, *16* (4), 211−213.
(39) Wang, C.; Langrock, C.; Marandi, A.; Jankowski, M.; Zhang, M.; Desiatov, B.; Fejer, M. M.; Lončar, M. Ultrahigh-Efficiency Wavelength Conversion in Nanophotonic Periodically Poled Lithium Niobate Waveguides. *Optica* **2018**, *5* (11), 1438−1441.
(40) Wegener, H. A. R.; R, H. A. The Gated-Access MNOS Memory Transistor. *IEEE Trans. Electron Devices* **1980**, *27* (1), 266−276.
(41) Gritsenko, V. A.; Morokov, Y. N.; Novikov, Y. N.; Xu, J. B. Memory Effect in Silicon Nitride in Silicon Devices. *arXiv:cond-mat/0011435* **2000**, na.
(42) Naich, M.; Rosenman, G.; Roizin, Y. Profiling of Deep Traps in Silicon Oxide-Nitride-Oxide Structures. *Thin Solid Films* **2005**, *471* (1−2), 166−169.
(43) Tzeng, S.-D.; Gwo, S. Charge Trapping Properties at Silicon Nitride/Silicon Oxide Interface Studied by Variable-Temperature Electrostatic Force Microscopy. *J. Appl. Phys.* **2006**, *100* (2), 023711.
(44) Vianello, E.; Perniola, L.; Blaise, P.; Molas, G.; Colonna, J. P.; Driussi, F.; Palestri, P.; Esseni, D.; Selmi, L.; Rochat, N.; et al. New Insight on the Charge Trapping Mechanisms of SiN-Based Memory by Atomistic Simulations and Electrical Modeling. In *2009 IEEE International Electron Devices Meeting (IEDM)*; IEEE, 2009; pp 1−4.
(45) Pfeiffer, M. H. P.; Liu, J.; Raja, A. S.; Morais, T.; Ghadiani, B.; Kippenberg, T. J. Ultra-Smooth Silicon Nitride Waveguides Based on the Damascene Reflow Process: Fabrication and Loss Origins. *Optica* **2018**, *5* (7), 884−892.
(46) Gouvêa, P. M. P.; Margulis, W. Annealing Experiments in Frequency-Doubling Fibers. *J. Opt. Soc. Am. B* **1994**, *11* (8), 1515−1518.
(47) Margulis, W.; Tarasenko, O.; Myrén, N. Who Needs a Cathode? Creating a Second-Order Nonlinearity by Charging Glass Fiber with Two Anodes. *Opt. Express* **2009**, *17* (18), 15534−15540.
(48) Dalton, L. R.; Sullivan, P. A.; Bale, D. H. Electric Field Poled Organic Electro-Optic Materials: State of the Art and Future Prospects. *Chem. Rev.* **2010**, *110* (1), 25−55.
(49) Nitiss, E.; Tokmakovs, A.; Pudzs, K.; Busenbergs, J.; Rutkis, M. All-Organic Electro-Optic Waveguide Modulator Comprising SU-8 and Nonlinear Optical Polymer. *Opt. Express* **2017**, *25* (25), 31036−31044.
(50) Bergot, M.-V.; Farries, M. C.; Fermann, M. E.; Li, L.; Poyntz-Wright, L. J.; Russell, P. S. J.; Smithson, A. Generation of Permanent Optically Induced Second-Order Nonlinearities in Optical Fibers by Poling. *Opt. Lett.* **1988**, *13* (7), 592−594.
(51) Camara, A. R.; Laurell, F.; Pereira, J. M. B.; Tarasenko, O.; Margulis, W. Linear Electro-Optical Effect in Silica Fibers Poled with Ultraviolet Lamp. *Opt. Express* **2019**, *27* (10), 14893−14902.
(52) Ikushima, A. J.; Fujiwara, T.; Saito, K. Silica Glass: A Material for Photonics. *J. Appl. Phys.* **2000**, *88* (3), 1201−1213.

DOI: 10.1021/acsphotonics.9b01301
ACS Photonics 2020, 7, 147−153